

ELEVENTH EUROPEAN ROTORCRAFT FORUM

Paper No. 83

INFLUENCE OF HIGH-ORDER DYNAMICS ON HELICOPTER  
FLIGHT-CONTROL SYSTEM BANDWIDTH

Robert T. N. Chen  
NASA Ames Research Center  
Moffett Field, California 94035 U.S.A.

and

William S. Hindson  
Stanford University  
Stanford, California 94305 U.S.A.

September 10-13, 1985

London, England

THE CITY UNIVERSITY, LONDON, EC1V OHB, ENGLAND

INFLUENCE OF HIGH-ORDER DYNAMICS ON HELICOPTER  
FLIGHT-CONTROL SYSTEM BANDWIDTH

Robert T. N. Chen  
NASA Ames Research Center  
Moffett Field, California 94035 U.S.A.

and

William S. Hindson  
Stanford University  
Stanford, California 94305 U.S.A.

Abstract

The increasing use of highly augmented digital flight-control systems in modern military helicopters has prompted an examination of the influence of rotor dynamics and other high-order dynamics on control-system performance. A study has been conducted to correlate theoretical predictions of feedback gain limits in the roll axis with experimental test data obtained from a variable-stability research helicopter. Feedback gains, the break frequency of the presampling sensor filter, and the computational frame time of the flight computer were systematically varied. The results, which showed excellent theoretical and experimental correlation, indicate that the rotor-dynamics, sensor-filter, and digital-data processing delays can severely limit the usable values of the roll-rate and roll-attitude feedback gains.

Nomenclature

- $A_{1c}$  = lateral cyclic pitch, deg  
 $a_1$  = longitudinal, first-harmonic, flapping coefficient, deg  
 $\dot{a}_1$  = time rate of change of  $a_1$ , deg/sec  
 $b_1$  = lateral, first-harmonic, flapping coefficient, deg  
 $\dot{b}_1$  = time rate of change of  $b_1$ , deg/sec  
 $e^{-\tau s}$  = transport delay of  $\tau$  sec  
 $K_p$  = roll-rate feedback gain, deg/deg/sec  
 $K_\phi$  = roll-attitude feedback gain, deg/deg  
 $p$  = roll rate, deg/sec (or rad/sec)  
 $q$  = pitch rate, deg/sec (or rad/sec)

$s$  = Laplace transform variable  
 $T_i$  = time constants of the actuator, sec  
 $u$  = longitudinal airspeed component in body axis, ft/sec  
 $v$  = lateral airspeed component in body axis, ft/sec  
 $\zeta$  = damping ratio  
 $\theta$  = pitch attitude, deg (or rad)  
 $\lambda$  = eigenvalue, 1/sec  
 $\sigma$  = real part of the eigenvalue, 1/sec  
 $\phi$  = roll attitude, deg (or rad)  
 $\omega$  = damped natural frequency, rad/sec  
 $\omega_n$  = undamped natural frequency, rad/sec  
 $\Omega$  = rotor rotational speed, rad/sec

## 1. Introduction

The operators of variable-stability research helicopters have long been aware of severe limitations in feedback gain settings when attempting to increase the bandwidth of flight-control systems needed to assure good fidelity during in-flight simulations. In a single-rotor helicopter, the effect of these high gains is to cause pitch and roll oscillations in the frequency range around 5 rad/sec; hence, this problem is of great concern in flight control. The problem is usually compounded by the need for severe filtering of feedback sensors to eliminate rotor system noise, and much effort is often devoted to designing compensation to reduce these effects (Ref. 1).

These limitations have also been encountered within the helicopter industry, where achievable stability augmentation system gains that actually result from development flight tests have often been far below values originally predicted. Now, with an increasing emphasis on high-bandwidth mission tasks, such as nap-of-the-earth flight and air combat for military helicopters, coupled with the development of new rotor systems and the trend toward using superaugmented, high-gain, flight-control systems (Ref. 2), to achieve good command-following, gust-disturbance rejection and insensitivity to parameter variations with flight conditions, there is a widespread need for improved understanding of these limitations.

Accordingly, a coordinated program involving analysis and flight testing was conducted to investigate the fundamental factors associated with the roll oscillation problem for a simple, high-gain, digital, lateral-control system. The analysis considered both a single-articulated-rotor helicopter (S-61), and a tandem-rotor helicopter (CH47). The characteristics in roll were shown to be strongly influenced by the rotor dynamics and the sensor filter characteristics, and were found to be very similar for both vehicles. The CH47 variable-stability research helicopter was used as the test vehicle to validate the analysis.

Of particular interest in the investigation were the influences of the rotor dynamics, the phase lags introduced by the sensor filters and servo actuators, and the transport delay associated with the on-board digital processor. The test helicopter provided an easy means for systematic variations in the feedback gains, presampling sensor filters, and computational frame time of the digital computer.

The analytical development, conduct of the flight tests, and data collection and reduction are described in the following sections, followed by a summary and discussion of the analytical and experimental results.

## 2. Analysis

### Influence of Rotor Dynamics on Helicopter Roll Response

Miller (Ref. 3) and Ellis (Ref. 4) were perhaps the first to point out the need to include the rotor dynamics in the analysis and design of high-gain attitude-stabilization systems for helicopters. Hall and Bryson (Ref. 5) also showed analytically that neglecting the rotor dynamics in the model used to design a high-performance hover autopilot using Linear-Quadratic-Gaussian (LQG) methodology can result in unstable closed-loop response of the more completely modeled system.

The potential for instability is associated with the regressing-flapping mode of the rotor (Fig. 1). When angular-rate or attitude feedback is increased, this root migrates towards a right-half plane zero in the open loop  $p/A_{1c}$  transfer function. This behaviour is investigated in detail for the S-61 in Ref. 6, but only the open-loop transfer function showing the participating pole-zero pair are included here (Table 1).

To investigate these phenomena experimentally, a coupled rotor-fuselage model of the CH47 helicopter was developed using the tip-path-plane modeling technique described in Refs. 7 and 8; these methods, which have been used to produce a generic single-rotor helicopter-simulation model (Ref. 8) were modified for this study to account for the tandem-rotor configuration. To simplify the state equations, the

horizontal translational velocities were neglected, as they have little effect on the roll oscillation problem.

Using this model for the CH47, the root-locus diagram for increasing values of roll-rate and roll-attitude feedback gains was determined using the stability and control matrices shown in Table 2. The results are also shown in Table 2, and they are plotted in Fig. 2. The effect of increasing the roll-rate feedback gain is to quickly increase the frequency and reduce the damping of the migrating mode, while increases in the roll-attitude gain act to rapidly destabilize the closed-loop system without much effect on frequency. The roll-rate gain for neutral stability is slightly larger than 3 deg/deg/sec. These results are similar to those obtained in Ref. 6 for the single-rotor S-61 helicopter. The open-loop roll-rate to lateral-cyclic transfer function was also calculated for the CH47 (Table 1) and the same migration of the regressing-flapping mode to the right-half plane zero was found to prevail. The remainder of this paper focuses on the roll dynamics of the CH47.

#### Influence of Sensor Filters, Servo Actuators, and Digital Delays

The simplified flight-control system and analysis model used in this study is shown in Fig. 3. The arrangement reflects some details of the test helicopter (to be discussed in a subsequent section). In general, the CH47 analysis model represents a conventional stability augmentation system (SAS) that uses an electrohydraulic series actuator to add rate damping and attitude stiffness to the pilot's mechanical control inputs. Nonlinearities such as actuator rate and authority limiting are not considered. Alternatively, this system contains the feedbacks usually found in model-following systems that have been used frequently in research helicopters, which are now being applied to advanced command augmentation systems for the next generation of military rotorcraft.

The analysis model also contains a noise-rejection filter on the roll-rate gyro signal, and a sampler and zero-order-hold (ZOH) representation of the digital processor. The requirement for the sensor filter is often overlooked in the design, analysis, or simulation of helicopter flight control systems, yet its effect on system bandwidth will be shown to be profound. In the CH47, the 3/rev rotor noise at 11 Hz has an amplitude averaging 1.8 deg/sec that must be attenuated prior to reaching the swashplate actuators via the  $K_p$  times  $p$  feedback structure. While compensation such as that proposed in Ref. 1 would normally be designed to somewhat offset the phase lag introduced by the sensor filter, none was included in this investigation.

This section examines the influence of the control system actuators, the filter breakpoint, and the transport delay of the digital processor on the CH47 roll-oscillation characteristics.

The implementation in the test aircraft allowed variations to be made easily in the digital-computer frame time, and the break frequency of the third-order Bessel filter used to remove 11-Hz (3/rev) rotor system noise from the roll-rate gyro signal. These parameters, along with the feedback gains, were used as the principal variables for evaluation. The nominal values of these parameters were 25 msec and 5 Hz, respectively. The servo actuators, modeled in Fig. 3 by first-order time constants, and the nominal 25-msec computer frame time, were represented by a combined transport delay of 75 msec. A first-order Padé approximation was used in the analysis to model the transport time delays.

Figure 4 shows the influence on the CH47 roll-axis dynamics when the 5-Hz filter and the 75-msec actuator plus digital transport delay are included in the analysis. The results indicate that the roll-rate gain limit is greatly reduced (by a factor of 6), compared to when rotor dynamics alone are modeled (Fig. 2), and the frequency of the roll oscillation is also greatly reduced.

The influence of various filter break frequencies is shown in Fig. 5, where the root loci of the roll-oscillation eigenvalues are plotted for filters with break frequencies of 10 Hz, 5 Hz, and 3.3 Hz. Even for the highest bandpass filter, the reduction in achievable roll-rate feedback gain compared to the case of rotor dynamics alone is dramatic. Of course, the 10-Hz filter would be impractical to implement by itself in the CH47 since there would be insufficient attenuation of the 11-Hz rotor system noise in the command signals to the actuators. The transfer functions for the three filters are shown in Table 3.

The combined effects of roll-rate and roll-attitude feedback on the roll-oscillation characteristics were examined for the 5-Hz and 3.3-Hz filters with the nominal computer frame time of 25 msec (40-Hz rate). The results are shown in Figs. 6 and 7. For a low-roll-rate feedback gain ( $K_p < 0.3$  deg/deg/sec), the roll-attitude gain is limited to about 1 deg/deg for the 5-Hz filter, and to significantly lower values at higher values of  $K_p$ . The gain limits for both  $K_p$  and  $K_\phi$  are reduced considerably with the 3.3-Hz filter, and as can be seen in Fig. 7, the frequency of the roll oscillation is also reduced.

The influence of the computer frame time was also examined. Fig. 8 shows the roll-oscillation characteristics when the computer frame time is increased to 62 msec (16-Hz rate). The characteristics with respect to the combined variations in  $K_p$  and  $K_\phi$  are similar to those presented in Fig. 7 for the shorter frame time with the 3.3-Hz filter. These two configurations have, in effect, an additional transport delay of 37 msec compared to the nominal configuration, showing the equivalent influence of additional delays in the closed loop, whatever their source.

These analyses were performed several months before the flight tests began. They were used to plan the tests and to correlate with the test data.

### 3. Flight Test Implementation and Data Collection

The aircraft used for the flight tests was the CH-47B variable-stability research helicopter operated at Ames Research Center. A brief description of the research system installed in this aircraft is contained in Ref. 8.

The flight-control system of this helicopter has been modified, relative to the basic CH-47B, to include full-authority, electrohydraulic, parallel actuators driven by control law signals generated in analog and digital flight computers. The motion of these actuators is transmitted through rotary clutches to the basic aircraft-control system at a summing link connected to the safety pilot's mechanical controls. Downstream from the summing link in the roll axis are "lower" boost and series SAS actuators, a control mixing box, and finally four "upper" boost actuators that transmit the roll-axis commands to the forward and aft swash plates. The hysteresis that undoubtedly exists in this extensive linkage was not modeled for this investigation. The time constants used for the individual actuators are shown in Fig. 3.

Safety monitoring equipment is installed to disengage the variable stability system automatically if the actuator rates exceed 66% of the hydraulic limit, thereby assuring linearity of operation. A "SAS-canceling" feature was used to remove the effects of the basic CH-47B stability augmentation system while testing the high-gain lateral-control system of this study.

The electrical implementation of the lateral-control system is shown in Fig. 3. Electrical control commands from the fly-by-wire controls in the right cockpit are scaled to provide "direct drive" of the basic CH-47B controls, but with roll-rate and roll-attitude terms of variable gain added. The digital computer was programmed to sample the input data at the desired frame interval and compute the direct control and the sensor feedback terms. The resulting command to the roll actuator was not output until the next sampling time, and this effective transport delay of a full frame was allowed for in the analysis. The pitch, yaw, and collective axes were programmed in the direct-drive mode only, with the SAS-canceling system selected off. Therefore, characteristics in those axes were those of the basic CH-47B.

Filters are usually incorporated at the inputs to the variable-stability system actuators to smooth the staircase commands from the digital processor, but in the roll axis the filter was removed for this investigation.

## Flight Test Procedure

The analysis proved to be very reliable for predicting the roll-rate and roll-attitude feedback gains required to induce oscillatory response. Together with the ease with which configurations could be varied in-flight, this predictive accuracy resulted in rapid data collection. More than 60 test points were obtained in four short flights. Because the system operator in the aircraft cabin could easily change the computer frame time, the feedback gains for the roll-rate and roll-attitude, and the analog filter characteristics in flight, more than 20 test points could often be accomplished during a single 1-hr flight.

After engaging the variable-stability system, a small pulse in the electric lateral controls was usually sufficient to excite the oscillation with a magnitude just below the trip threshold of the control-rate monitoring system. Neutrally damped, or mildly divergent configurations typically did not require any control input for excitation. Individual test runs lasted for 3 to 15 sec, depending on the damping involved, and motion amplitudes were typically very small and never of concern.

## Data Reduction

The flight-test data were recorded on magnetic tapes, and were reduced by measuring the damped or undamped frequency directly from an expanded time history of the oscillation. The damping was determined by comparing successive peaks in the response, which was assumed to arise from a single second-order mode.

## 4. Test Results

In this section, analytical and experimental results are compared for three test configurations: (1) the nominal configuration (25-msec computer frame time, 5-Hz filter breakpoint); (2) the reduced filter breakpoint (3.3 Hz); and (3) the increased computer frame time (62 msec).

### Nominal Configuration

The results from 23 flight-test points are compared directly with corresponding analytical points in Table 4. The agreement is extremely good. A graphical comparison of selected points, including their flight-test time histories, is presented in Fig. 9. Point A in Fig. 9 is a configuration ( $K_p = 0.7$ ,  $K_\phi = 0$ ) characterized by moderately high frequency and negative damping. The measured characteristics were  $\omega = 8$  rad/sec,  $\zeta = -0.045$ . These agree well with the calculated values of  $\omega = 7.9$  rad/sec,  $\zeta = -0.08$  shown in Table 4. Similarly, points B and C in Fig. 9, along with their respective time histories, are to be compared with the corresponding analytical points noted in Table 4.

### Reduced Filter Break Frequency

The 13 flight-test points that were used to document the 3.3-Hz filter configuration are compared in Table 5. Selected test points are shown graphically in Fig. 10. With this filter incorporated, lower frequencies characterize the oscillation and lower gains must be used. The test results indicated somewhat lower frequencies than were predicted, but the gain limits compared favorably.

### Increased Computer Frame Time

Twelve different configurations were tested using a computer frame time of 62 msec. The data are presented in Table 6 and in Fig. 11. Similar to the 3.3-Hz filter configuration, the predicted frequencies are about 10% higher than measured, although this discrepancy diminishes for lower frequency cases. However, predicted values of the feedback gains that define the stability boundary are in good agreement.

Four roll-rate time histories corresponding to stable and unstable configurations at both high and low frequencies are shown in Fig. 12. The configuration parameters are noted on the figure, and the correlation of the experimental results with the analysis is found in Table 6.

## 5. Discussion of the Results

In general, the flight-test data confirmed the analytic predictions with excellent accuracy, particularly considering the simplicity of the model. The stability limits for the roll-rate and the roll-attitude feedback gains used in the simplified high-gain flight-control system under investigation correlated extremely well with the theoretical predictions. However, the predicted frequency of the roll oscillation tended to be somewhat higher (at most 10%) than was measured in the flight tests.

A cause for these discrepancies might be the Padé approximation. While this is a good representation for a pure time delay at lower frequencies, it becomes less accurate as frequency increases. Other explanations for the discrepancies may be the models used for the servo actuators, and the hysteresis that undoubtedly is present in the control system linkage. An additional factor for consideration is the influence of dynamic inflow (Refs. 10 and 11).

Interpreting the test results in the context of the simple lateral-control system used as the basis for this study, the roll-rate and roll-attitude feedback gains must be limited to less than about 0.25 deg/deg/sec and 0.4 deg/deg, respectively, for the CH47 configuration if the damping of the roll oscillation mode is to be kept above 0.3. This suggests that the bandwidth of an attitude command system in

the roll axis would be limited to about 2.4 rad/sec in hover unless appropriate compensation was added.

## 6. Conclusions

This paper has discussed a combined analytical and experimental program conducted to investigate the fundamental factors associated with the roll oscillation program for a simple, high-gain, digital, lateral-control system. The analysis was performed using a simplified coupled rotor-fuselage model of the CH47 helicopter in hover and examined the roll dynamics as influenced by the rotor dynamics, the phase lags introduced by the sensor filters and servo actuators, and the transport delay associated with the on-board digital processor. Flight-test data were obtained with a variable-stability CH47 research helicopter to verify the results of the analysis. The results of the investigation show that

(1) the roll-oscillation phenomena associated with a high-gain, digital, flight-control system can be predicted satisfactorily for hover with a relatively simple analytical model, and that

(2) rotor dynamics, sensor filters, and digital data-processing delays can severely limit the usable values of the feedback gains, and thus the bandwidth of the control system.

## References

- 1) Garren, J. F., Jr. et al., The Application of a Modified Complementary Filtering Technique for Increased Aircraft Control System Frequency Bandwidth in a High Vibration Environment, NASA TM X-74040, 1977.
- 2) McRuer, D. et al., A Perspective on Superaugmented Flight Control Advantages and Problems, presented at AGARD Conference on Active Control, Ontario, Canada, Oct. 1984.
- 3) Miller, R. H., A Method for Improving the Inherent Stability and Control Characteristics of Helicopters, J. Aeronautical Sciences, June 1950, pp. 363-374.
- 4) Ellis, C. W., Effects of Articulated Rotor Dynamics on Helicopter Automatic Control System Requirements, Aeronautical Engineering Review, July 1953, pp. 30-38.
- 5) Hall, W. E., Jr. et al., Inclusion of Rotor Dynamics in Controller Design, J. Aircraft, 10, (4), Apr. 1973, pp. 200-206.
- 6) Chen, R. T. N. et al., Analytical and Flight Investigation of the Influence of Rotor and Other High-Order Dynamics on Helicopter Flight-Control System Bandwidth, NASA TM 86696, 1985.

- 7) Chen, R. T. N., Effects of Primary Rotor Parameters on Flapping Dynamics, NASA TP-1431, 1980.
- 8) Talbot, P. D. et al., A Mathematical Model of a Single Main Rotor Helicopter for Piloted Simulation, NASA TM-84281, Sept. 1982.
- 9) Kelly, J. R. et al., Description of the VTOL Approach and Landing Technology (VALT) CH-47 Research System, NASA TP-1436, Aug. 1979.
- 10) Ormiston, R. A., Application of Simplified Inflow Models to Rotorcraft Dynamic Analysis, J. AHS, July 1976, pp. 34-37.
- 11) Pitt, D. M. et al., Theoretical Prediction of Dynamic-Inflow Derivatives, Vertica, 5, 1981, pp. 21-34.

Table 1. Pole-zero location of  $p/A_{1c}$  transfer functions in hover.<sup>a</sup>


---



---

S-61 (Rotor dynamics included; body with  $p, q, \phi, \theta, u,$  and  $v$  as state variables)

$$\frac{p}{A_{1c}}(s) = \frac{4.970(0)(-0.002)(-0.703)(-13.246)(-55.420)(0.40; -0.31)[47.91; -0.11]}{(0.38; -0.29)(0.50; -0.08)(1.24; 0.98)(14.23; 0.91)[40.73; 0.39]}$$

CH47 (Rotor dynamics included; body with  $p, q$  as state variables)

(a) Body + rotor

$$\frac{p}{A_{1c}}(s) = \frac{4.722(-1.083)(-12.987)(-61.112)[38.449; -0.291]}{(1.184; 0.988)(12.792; 0.954)[46.499; 0.284]}$$

(b) Body + rotor + filter

$$\frac{p}{A_{1c}}(s) = \frac{146188.3(-1.083)(-12.987)(-61.112)[38.449; -0.291]}{(1.184; 0.988)(12.792; 0.954)(46.499; 0.284)(-29.576)[32.559; 0.724]}$$

5 Hz, 3rd order  
Bessel filter

---



---

<sup>a</sup>( $\lambda$ ) for real eigenvalues; ( $\omega_n; \zeta$ ) for complex eigenvalues.  
[ ] = pole-to-zero migration pairs.

Table 2. Stability and control matrices, and eigenvalues of closed-loop system of the CH47 in hover.

$$\frac{d}{dt} x = Fx + Gu, \quad x = (\dot{a}_1 \dot{b}_1 a_1 b_1 q p)^T, \quad \underline{u} = A_{1c}$$

$$F = \begin{bmatrix} -25.9160 & -48.1700 & -20.7090 & -624.1740 & -25.9160 & -49.8900 \\ 48.1700 & -25.9160 & 624.1740 & -20.7090 & 49.8900 & -20.9160 \\ 1.0000 & 0.0000 & 0.0000 & 0.0000 & 0.0000 & 0.0000 \\ 0.0000 & 1.0000 & 0.0000 & 0.0000 & 0.0000 & 0.0000 \\ -0.0640 & 0.0000 & 1.6320 & 0.0000 & -0.9350 & 0.0000 \\ 0.0000 & -0.3790 & 0.0000 & 9.7200 & 0.0000 & -0.3790 \end{bmatrix} \quad G = \begin{bmatrix} 624.1740 \\ 0.0000 \\ 0.0000 \\ 0.0000 \\ 0.0000 \\ 4.7220 \end{bmatrix}$$


---

$K_p$  (deg/deg);  $K_\phi = 0$

|  | 0             | 0.1           | 0.3           | 0.5           | 1.0           | 2.0           | 3.0           | 4.0           | 5.0           |
|--|---------------|---------------|---------------|---------------|---------------|---------------|---------------|---------------|---------------|
|  | -13.19±j44.59 | -13.53±j44.43 | -14.24±j44.12 | -14.99±j43.82 | -17.03±j43.11 | -21.70±j42.33 | -26.34±j42.58 | -30.47±j43.33 | -34.15±j44.17 |
|  | -12.21±j3.82  | -11.04±j3.86  | -7.23±j6.38   | -6.43±j9.38   | -5.23±j14.14  | -2.75±j19.91  | -0.41±j23.12  | 1.39±j25.06   | 2.73±j26.39   |
|  | -1.17±j0.18   | -3.36         | -10.52        | -11.58        | -12.26        | -12.61        | -12.73        | -12.79        | -12.83        |
|  |               | -1.10         | -1.09         | -1.09         | -1.09         | -1.08         | -1.08         | -1.08         | -1.08         |

83-12

Table 3. Transfer functions of three third-order Bessel filters.

$$T_B(s) = \frac{a_0}{s^3 + a_2 s^2 + a_1 s + a_0} \doteq e^{-\tau s}$$

| Break frequency (Hz) | $a_0$     | $a_1$   | $a_2$  | $\tau$ (sec) |
|----------------------|-----------|---------|--------|--------------|
| 3.3                  | 9186.85   | 1081.74 | 50.95  | 0.115        |
| 5.0                  | 30959.14  | 2431.48 | 76.39  | 0.078        |
| 10.0                 | 247673.12 | 9725.92 | 152.78 | 0.039        |

Table 4. Comparison of theoretical calculation and flight-test results for the roll oscillation mode  
 [40-Hz frame rate (or 25-msec frame time); 5-Hz Bessel filter].

| $K_{\phi}$<br>(deg/deg) | 0          |        | 0.2    |        | 0.5    |        | 0.7    |       | 0.8    |       | 0.9    |        | 1.0    |        | 1.2    |        | 1.4    |        |       |
|-------------------------|------------|--------|--------|--------|--------|--------|--------|-------|--------|-------|--------|--------|--------|--------|--------|--------|--------|--------|-------|
|                         | Theory     | Test   | Theory | Test   | Theory | Test   | Theory | Test  | Theory | Test  | Theory | Test   | Theory | Test   | Theory | Test   | Theory | Test   |       |
| 0.1                     | $\omega =$ |        |        |        | 3.21   | 2.8    |        |       | 3.84   | 3.6   |        |        | 4.14   | 3.9    | 4.15   | 4.15   |        |        |       |
|                         | $\zeta =$  |        |        |        | 0.232  | 0.15   |        |       | 0.055  | 0.08  |        |        | -0.015 | 0.02   | -0.067 | -0.05  |        |        |       |
| 0.2                     | $\omega =$ | 5.25   | Stable |        |        | 4.65   | 4.65   |       |        | 4.79  | 4.5    |        |        | 4.95   | 4.2    | 5.10   | 4.6    | 5.26   | 4.8   |
|                         | $\zeta =$  | 0.444  |        |        |        | 0.276  | 0.25   |       |        | 0.117 | 0.10   |        |        | 0.039  | 0.05   | -0.021 | -0.02  | -0.069 | -0.07 |
| 0.3                     | $\omega =$ | 6.19   | Stable |        |        |        |        |       |        |       |        |        |        |        |        |        |        |        |       |
|                         | $\zeta =$  | 0.255  |        |        |        |        |        |       |        |       |        |        |        |        |        |        |        |        |       |
| 0.4                     | $\omega =$ | 6.79   | 6.4    |        |        | 6.58   | 6.6    | 6.54  | 5.5    |       |        | 6.51   | 5.8    | 6.51   | 5.9    | 6.52   | 5.9    | 6.55   | 6.0   |
|                         | $\zeta =$  | 0.132  | 0.1    |        |        | 0.054  | 0.10   | 0.019 | 0.15   |       |        | -0.016 | 0.06   | -0.033 | 0.08   | -0.066 | 0.0    | -0.096 | -0.10 |
| 0.5                     | $\omega =$ | 7.23   | 6.6    |        |        |        |        |       |        |       |        |        |        |        |        |        |        |        |       |
|                         | $\zeta =$  | 0.044  | 0.09   |        |        |        |        |       |        |       |        |        |        |        |        |        |        |        |       |
| 0.6                     | $\omega =$ | 7.59   | 7.4    | 7.57   | 7.4    | 7.51   | 7.5    |       |        |       |        |        |        |        |        |        |        |        |       |
|                         | $\zeta =$  | -0.024 | 0.025  | -0.047 | 0.0    | -0.076 | -0.06  |       |        |       |        |        |        |        |        |        |        |        |       |
| 0.7                     | $\omega =$ | 7.88   | 8.0    |        |        |        |        |       |        |       |        |        |        |        |        |        |        |        |       |
|                         | $\zeta =$  | -0.078 | -0.045 |        |        |        |        |       |        |       |        |        |        |        |        |        |        |        |       |

Table 5. Comparison of theoretical calculation and flight-test results  
 [40-Hz frame rate (or 25-msec frame time); 3.3-Hz Bessel filter].

| $K_{\phi}$<br>(deg/deg) | 0          |        | 0.3    |       | 0.5    |        | 0.8    |        | 1.0    |       |
|-------------------------|------------|--------|--------|-------|--------|--------|--------|--------|--------|-------|
| $K_p$<br>(deg/deg/sec)  | Theory     | Test   | Theory | Test  | Theory | Test   | Theory | Test   | Theory | Test  |
| 0.1                     | $\omega =$ |        |        |       | 3.33   | 3.2    | 3.89   | 3.7    | 4.17   | 4.0   |
|                         | $\zeta =$  |        |        |       | 0.195  | 0.20   | 0.024  | 0.01   | -0.043 | -0.05 |
| 0.2                     | $\omega =$ |        |        |       | 4.68   | 4.2    | 4.77   | 4.3    | 4.91   | 4.5   |
|                         | $\zeta =$  |        |        |       | 0.172  | 0.13   | 0.039  | 0.05   | -0.026 | -0.02 |
| 0.3                     | $\omega =$ | 5.67   | 5      |       |        |        |        |        |        |       |
|                         | $\zeta =$  | 0.19   | 0.2    |       |        |        |        |        |        |       |
| 0.4                     | $\omega =$ | 6.15   | 5.7    | 6.07  | 5.6    | 6.05   | 5.62   | 6.06   | 5.6    |       |
|                         | $\zeta =$  | 0.073  | 0.1    | 0.019 | 0.03   | -0.018 | -0.01  | -0.072 | -0.03  |       |
| 0.5                     | $\omega =$ | 6.50   | 5.85   |       |        |        |        |        |        |       |
|                         | $\zeta =$  | 0.011  | 0.02   |       |        |        |        |        |        |       |
| 0.6                     | $\omega =$ | 6.78   | 6.2    |       |        |        |        |        |        |       |
|                         | $\zeta =$  | -0.074 | -0.05  |       |        |        |        |        |        |       |

Table 6. Comparison of theoretical calculation and flight-test results  
 [16-Hz frame rate (or 62-msec frame time); 5-Hz Bessel filter].

| $K_\phi$<br>(deg/deg)  | 0          |        | 0.5        |        | 0.7    |        | 0.8    |       | 1.0    |        |       |
|------------------------|------------|--------|------------|--------|--------|--------|--------|-------|--------|--------|-------|
| $K_D$<br>(deg/deg/sec) | Theory     | Test   | Theory     | Test   | Theory | Test   | Theory | Test  | Theory | Test   |       |
| 0.1                    | $\omega =$ |        | 3.21       | 3.0    | 3.58   | 3.5    | 3.73   | 3.5   |        |        |       |
|                        | $\zeta =$  |        | 0.158      | 0.15   | 0.03   | 0.03   | -0.015 | -0.07 |        |        |       |
| 0.2                    | $\zeta =$  | 4.99   | unreadable | 4.44   | 3.9    |        |        | 4.56  | 4.2    | 4.69   | 4.3   |
|                        | $\zeta =$  | 0.374  |            | 0.179  | 0.16   |        |        | 0.027 | 0.0    | -0.046 | -0.07 |
| 0.4                    | $\omega =$ | 6.27   | 5.6        | 6.03   | 5.4    | 5.99   | 5.3    |       |        |        |       |
|                        | $\zeta =$  | 0.07   | 0.09       | -0.016 | -0.01  | -0.054 | -0.07  |       |        |        |       |
| 0.5                    | $\omega =$ | 6.63   | 6.05       |        |        |        |        |       |        |        |       |
|                        | $\zeta =$  | -0.016 | 0.0        |        |        |        |        |       |        |        |       |
| 0.6                    | $\omega =$ | 6.92   | 6.2        |        |        |        |        |       |        |        |       |
|                        | $\zeta =$  | -0.082 | -0.1       |        |        |        |        |       |        |        |       |

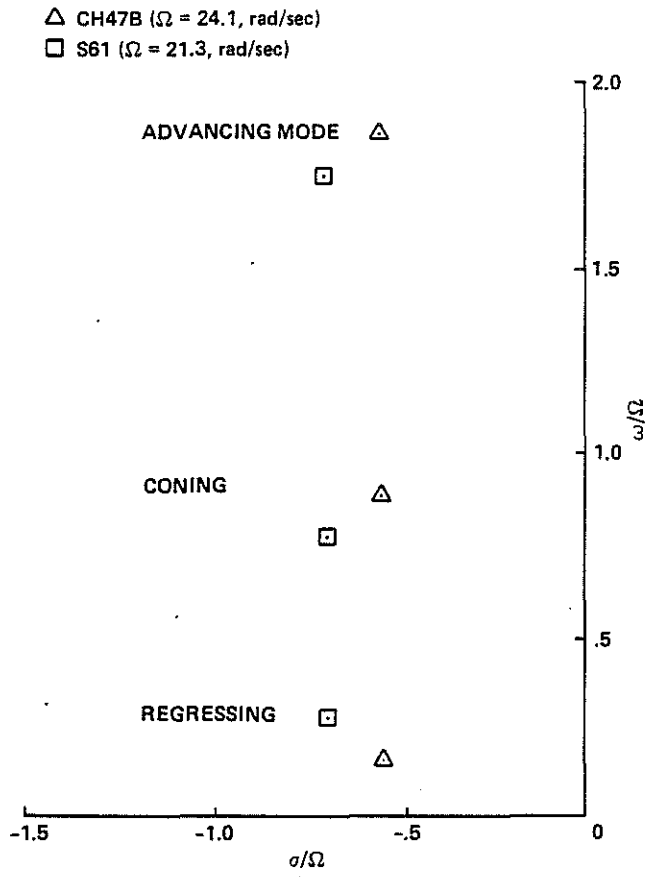


Fig. 1 Tip-path-plane modes for S-61 and CH47B at hover.

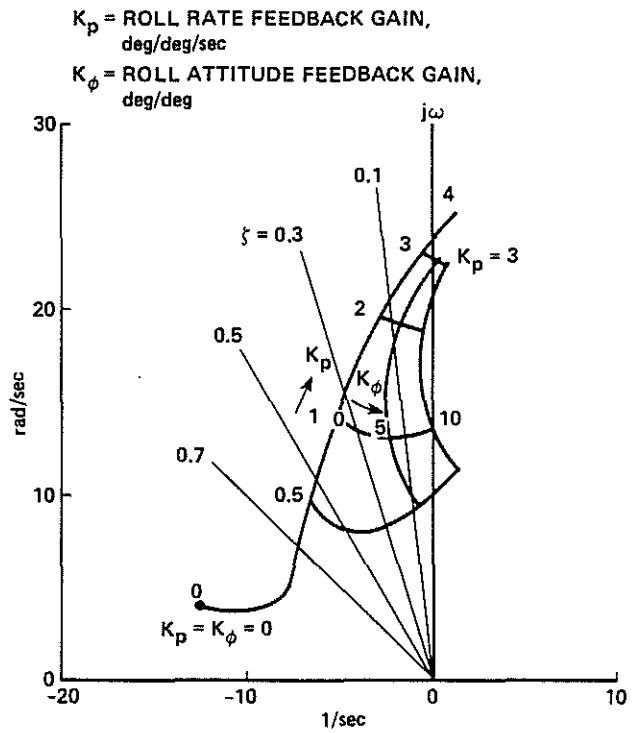


Fig. 2 Effect of rotor dynamics, CH47 at hover.

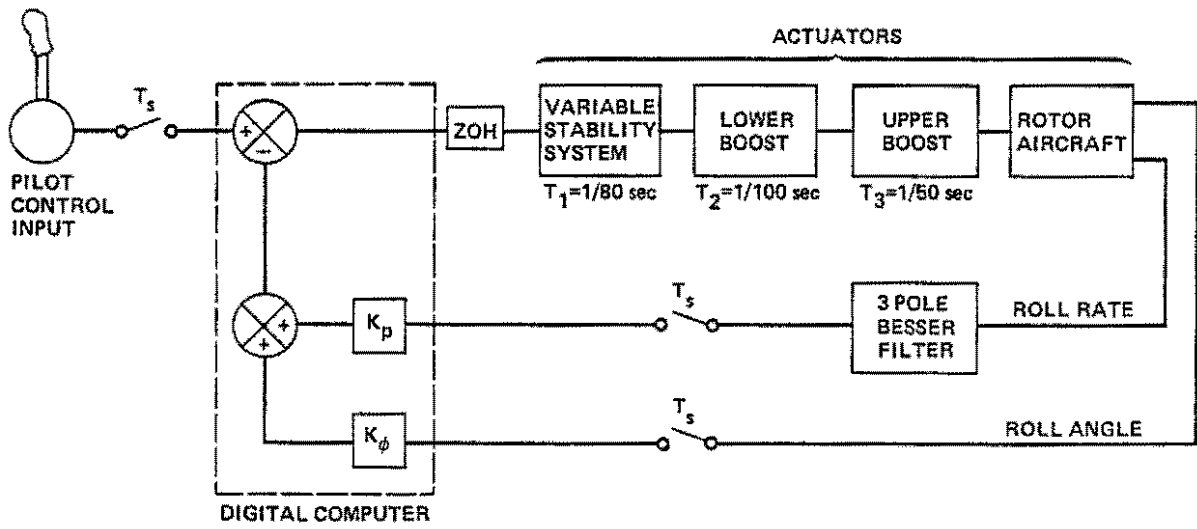


Fig. 3 CH47 analysis model.

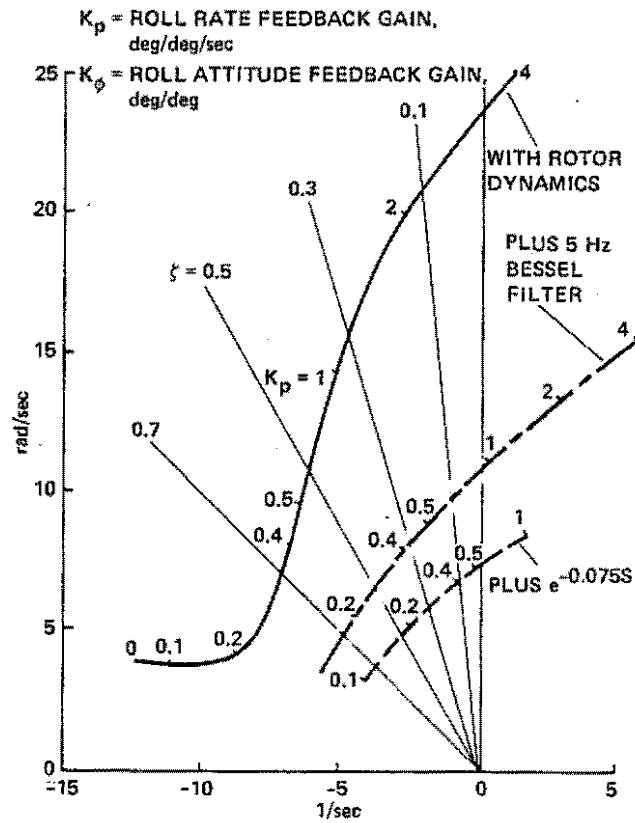


Fig. 4 Theoretical prediction of roll oscillation for the CH47B variable-stability helicopter.

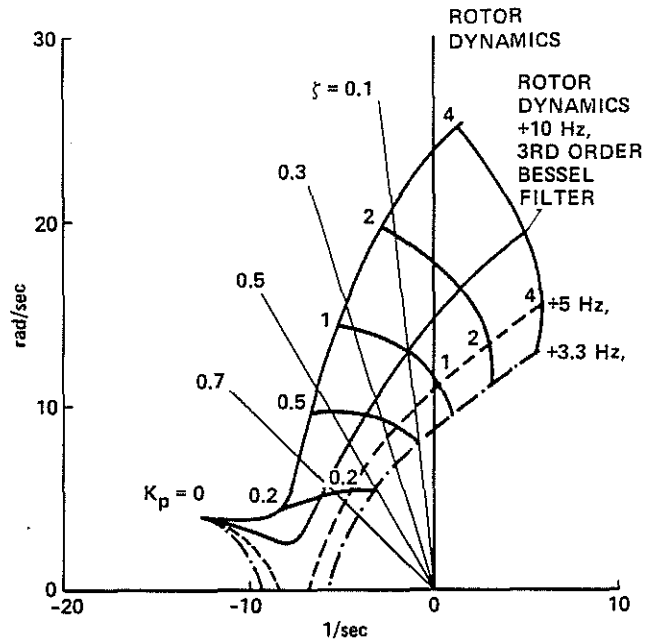


Fig. 5 Effect of rotor dynamics and roll-rate filter with varying break frequency (CH47).

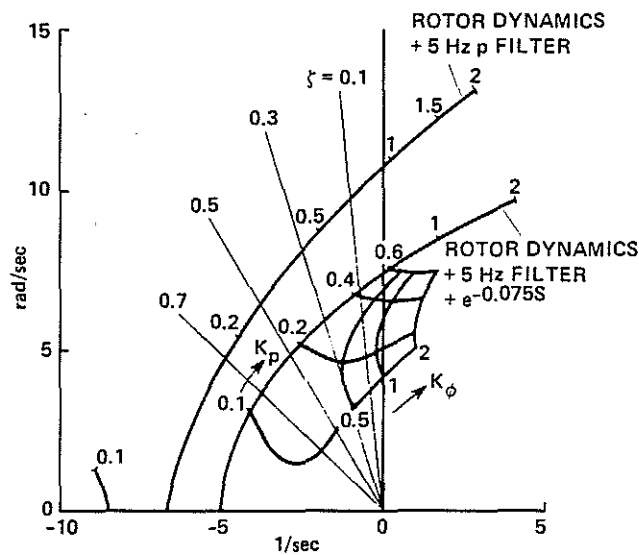


Fig. 6 Combined effect of  $K_p$  and  $K_\phi$  feedback for 25-msec frame time and 5-Hz roll-rate filter.

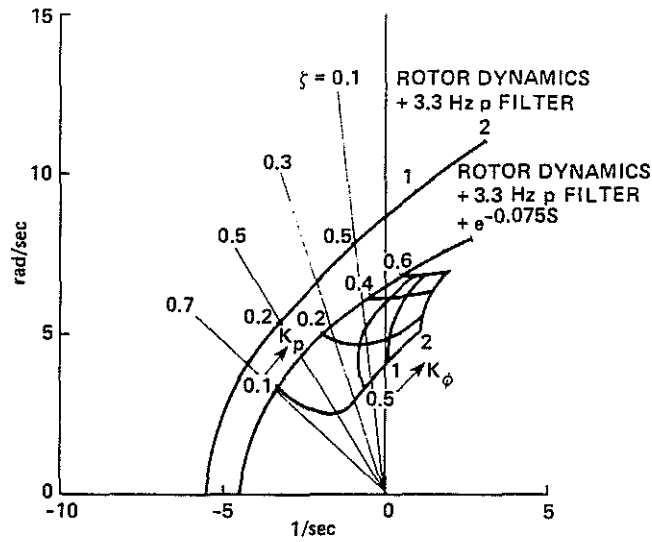


Fig. 7 Combined effect of  $K_p$  and  $K_\phi$  feedback for 25-msec frame time and 3.3-Hz roll-rate filter.

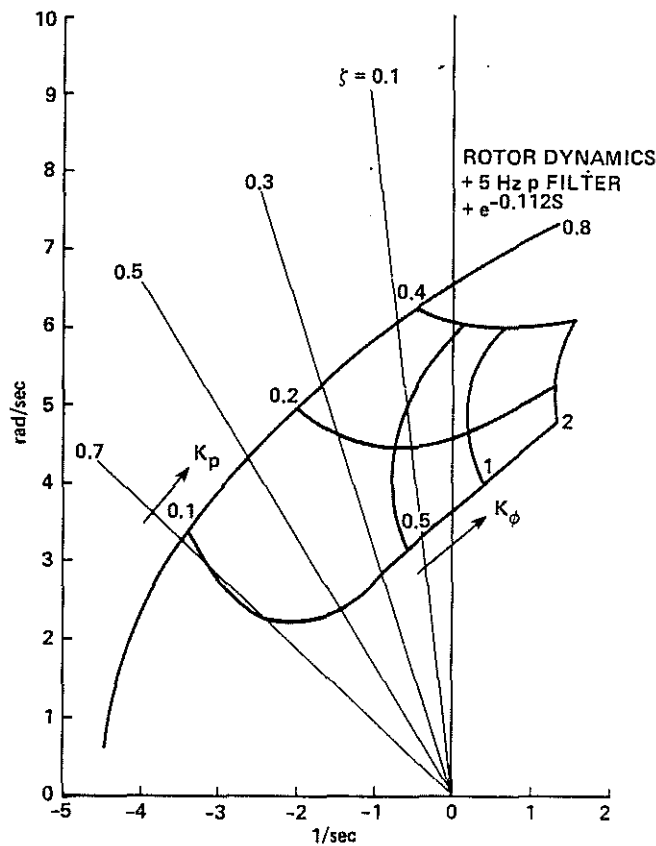


Fig. 8 Combined effect of  $K_p$  and  $K_\phi$  feedback for 62-msec frame time and 5-Hz roll-rate filter.

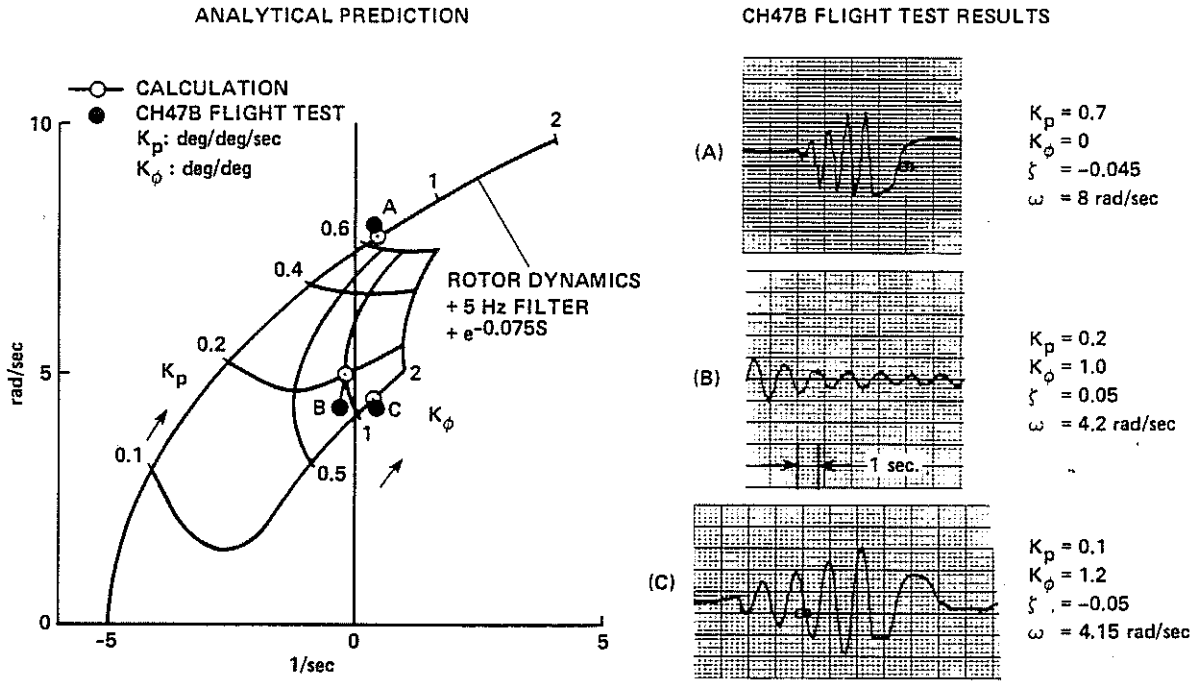


Fig. 9 Comparison of calculated and CH47B flight-test results at three different points: 25-msec frame time, 5-Hz roll-rate filter.

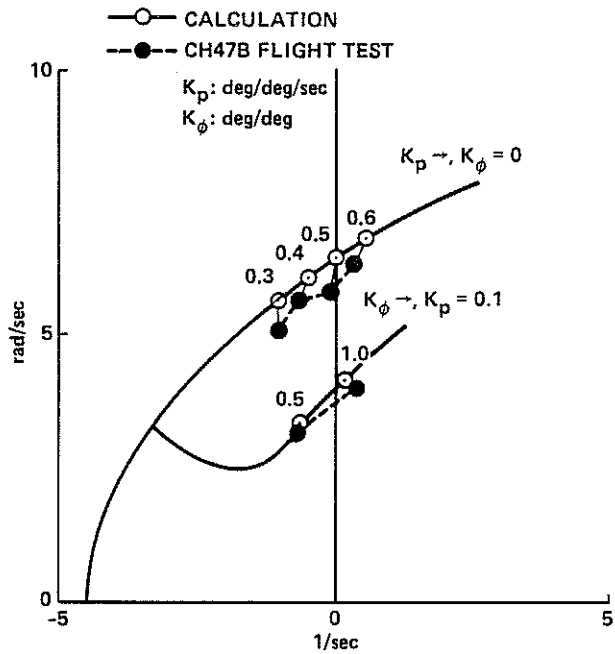


Fig. 10 Comparison of calculated and CH47B flight-test results: 25-msec frame time, 3.3-Hz roll-rate filter.

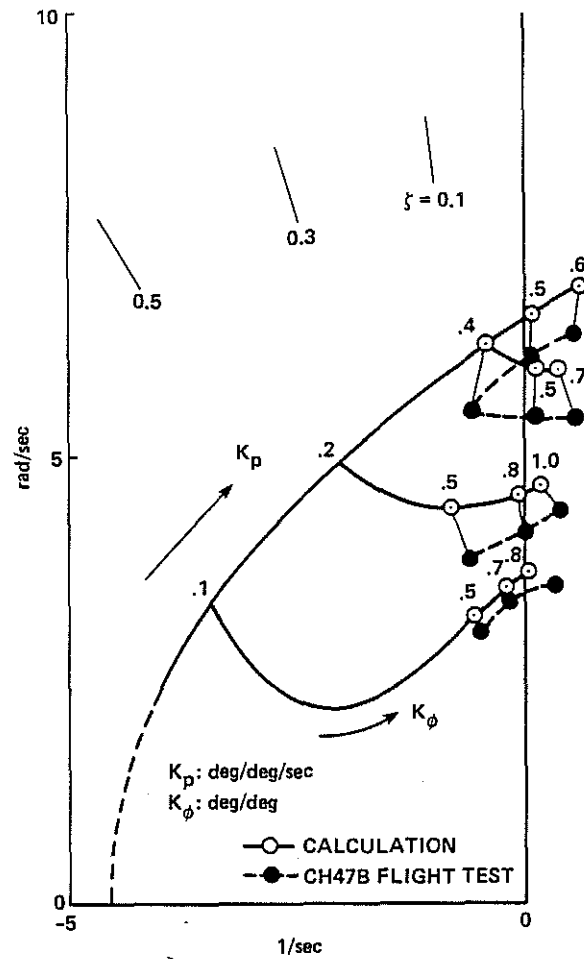


Fig. 11 Comparison of calculated and CH47B flight-test results: 62-msec frame time, 5-Hz roll-rate filter.

- 16 Hz FRAME RATE
- 5 Hz p FILTER

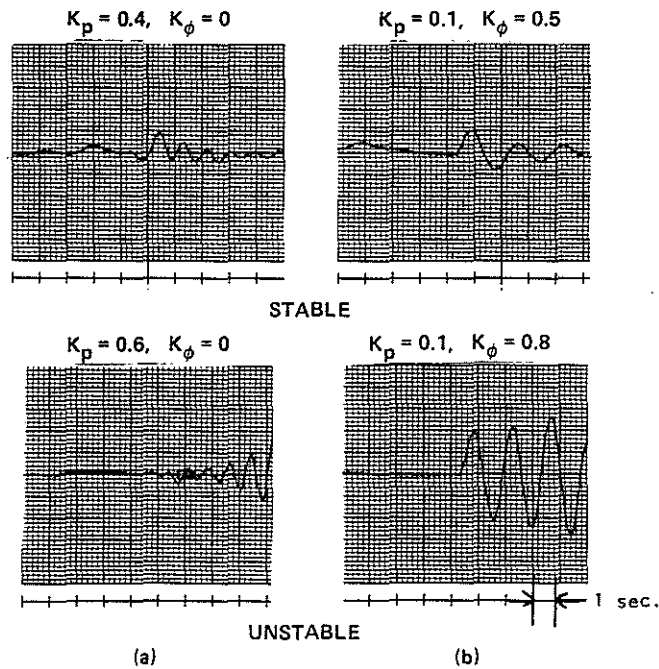


Fig. 12 Sample roll-oscillation time histories from CH47 flight test: 62-msec frame time, 5-Hz roll-rate filter.